

Supplementary Information

Hydrophilic engineering of VO_x-based nanosheets for ambient electrochemical ammonia synthesis at neutral pH

Wei Fang, Jin Zhao, Tao Wu, Yinjuan Huang, Lan Yang, Chuntai Liu, Qichun Zhang, Kevin Huang and Qingyu Yan

S1. Density functional theory calculations

All ground-state electronic calculations were performed by Perdew-Burke-Ernzerhof (PBE) generalized gradient approximation (GGA) exchange-correlation implemented in the Vienna *ab Initio* Simulation Package (VASP).^[S1-S3] The calculations use the projector augmented wave (PAW) method and valence configurations include the H (1s¹), O (2s²2p⁴), N (2s²2p³) and V (3p⁶3d⁴4s¹) states.^[S4,S5] Electronic structure was described within a plane-wave basis with a kinetic energy cut-off of 400 eV. For thermodynamic calculations such as lattice parameters and total energy, we employed the DFT+U formalism of Anisimov *et al.* to account for strong on-site Coulombic interactions of the V 3d-electrons, with a specific on-site potential of U = 3.25 eV.^[S6] Apart from that, electron spin-polarization is considered for all thermodynamic and electronic structure calculation, which is necessary for open-shell system. The lattice constants and atomic positions were both fully relaxed until a maximum energy difference and residual force on atoms converge were reached at 10⁻⁴ eV and 0.1 eV/Å, respectively. The Brillouin zone was sampled with 2×4×1. The DFT-D3 correction method was considered for van der Waals interactions and climbing-image nudged elastic band (CI-NEB) method was used to describe barrier of H₂O dissociation on mVO_x (V₂O₅ with oxygen vacancy) surface.^[S7,S8] The free energy profile for electrochemical reduction of N₂ to NH₃ on mVO_x surface was computed from:

$$\Delta G = \Delta E + \Delta E_{ZPE} - T\Delta S$$

Where ΔE , ΔE_{ZPE} , and $T\Delta S$ are the total energy difference, zero-point energy difference and the entropy difference between the adsorbed state and the gas phase, respectively. The total energy difference could be obtained from standard DFT calculations. The zero-point energy and the entropy can be obtained from vibrational frequencies derived from Hessians calculated from analytic gradients on adsorbates on V₂O₅ surface. The entropies and vibrational frequencies of molecules in the gas phase are taken from the NIST database. [<http://cccbdb.nist.gov/>]

S2. Turnover frequency estimation

To cross check our experimental results with theoretical predictions, we estimate turnover frequency (TOF) value from experiment and compare with the theoretical value. The specific capacitance is used to obtain electrochemical active surface area (ECSA). The specific capacitance for VO_x based electrode is about 1.636 mF cm⁻² and the specific capacitance for a flat surface is generally found to be about 20~60 μF cm⁻². Additionally, a Correction Factor (CF) is taken into consideration when using carbon cloth as substrate, and S denotes the

electrode area. Based on this value, we can estimate the ECSA of VO_x based electrode as following:

$$ECSA_{VO_x} = \frac{1.636 \text{ mF cm}^2}{20 \mu\text{F cm}^{-2}} \times S \times CF = 81.8 \times S \times CF \text{ cm}^2$$

The total number of NH₃ turnover rate (X_{NH_3}) at a given current (i) is calculated by:

$$X_{NH_3} = (|i| \text{ mA}) \left(\frac{1 \text{ C s}^{-1}}{1000 \text{ mA}} \right) \left(\frac{1 \text{ mol e}^{-1}}{96485.3 \text{ C}} \right) \left(\frac{1 \text{ mol NH}_3}{3 \text{ mol e}^{-1}} \right) \left(\frac{6.022 \times 10^{23} \text{ NH}_3 \text{ molecules}}{1 \text{ mol NH}_3} \right) \times 2.08 \times 10^{15} \frac{\text{NH}_3 \text{ molecules}}{\text{S}}$$

Since the O vacancy is considered as the active sites for the enhanced NRR performance, the active sites per surface area can be estimated by:

$$X_{\text{active sites}} = \left(\frac{0.96 O_{\text{vac}}/\text{unitcell}}{952.22 \text{ \AA}^3/\text{unitcell}} \right)^{2/3} = 1.0 \times 10^{14} O_{\text{vac}} \text{ cm}^{-2}$$

Among them, 0.96 is the estimated number of O vacancies per unit-cell based on the XPS analysis (the ratio of V⁴⁺/V⁵⁺ is 0.12) and the volume of the unit-cell is 952.22 Å³. For TOF of NH₃ yield can be calculated by:

$$TOF = \frac{2.08 \times 10^{15} \frac{\text{NH}_3}{\text{S}} \times |j|}{1.0 \times 10^{14} \text{ atoms cm}^{-2} \times 81.8 \times CF \text{ cm}^2}$$

Where $|j|$ denotes the NH₃ Faradaic current density contributed from oxygen vacancies ($|j|=|i|/S$).

In theory, TOF can be estimated from DFT calculations by:

$$r = \nu \exp\left(\frac{- (E_{act} + eU)}{k_B T}\right)$$

The E_{act} is the activation barrier for the rate limiting process, which is equal to 1.70 eV. It is reasonable to believe that there is ±0.3 eV uncertainty for DFT calculations. If we use a typical pre-factor ν on the order 10¹³,^[S9] an activation barrier E_{act} of 1.70 eV, and a potential around -0.35 V vs reversible hydrogen electrode (RHE) as reported in the experiment, a turnover rate is found to be as high as ~10⁻⁴ s⁻¹ which is close to the experiment result of ~10⁻³- 10⁻⁴ s⁻¹.

S3. Supporting figures

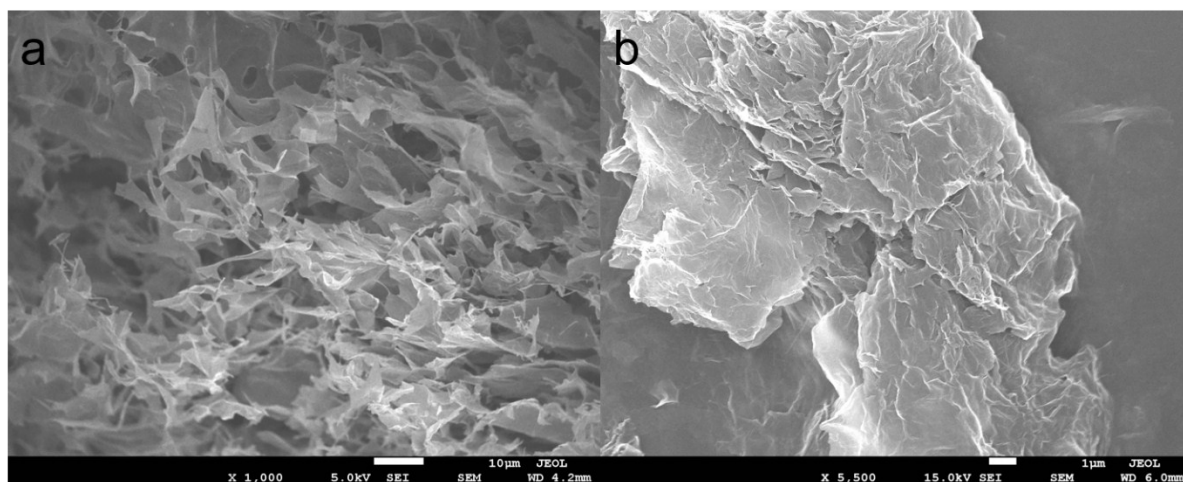


Fig. S1 SEM images of a) V_2O_5 nanosheet and b) mVO_x -rGO composite.

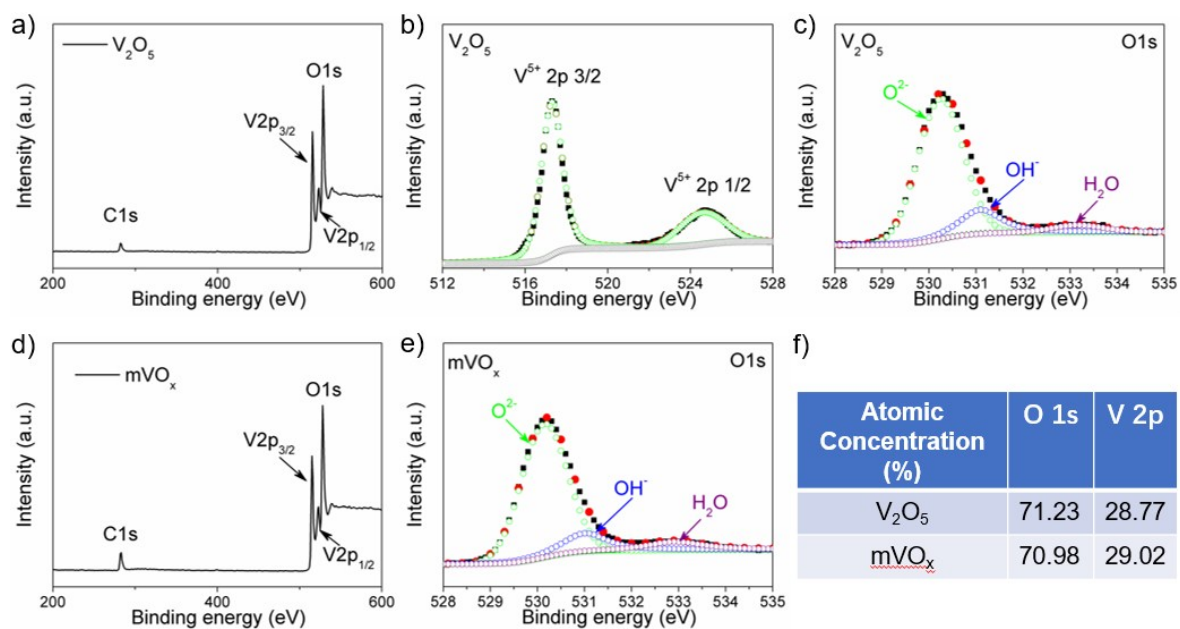


Fig. S2 XPS spectra of V_2O_5 from a) overview, b) V 2p, c) O1s and mVO_x from d) overview, e) O1s. f) Atomic concentrations of V_2O_5 and mVO_x by XPS.

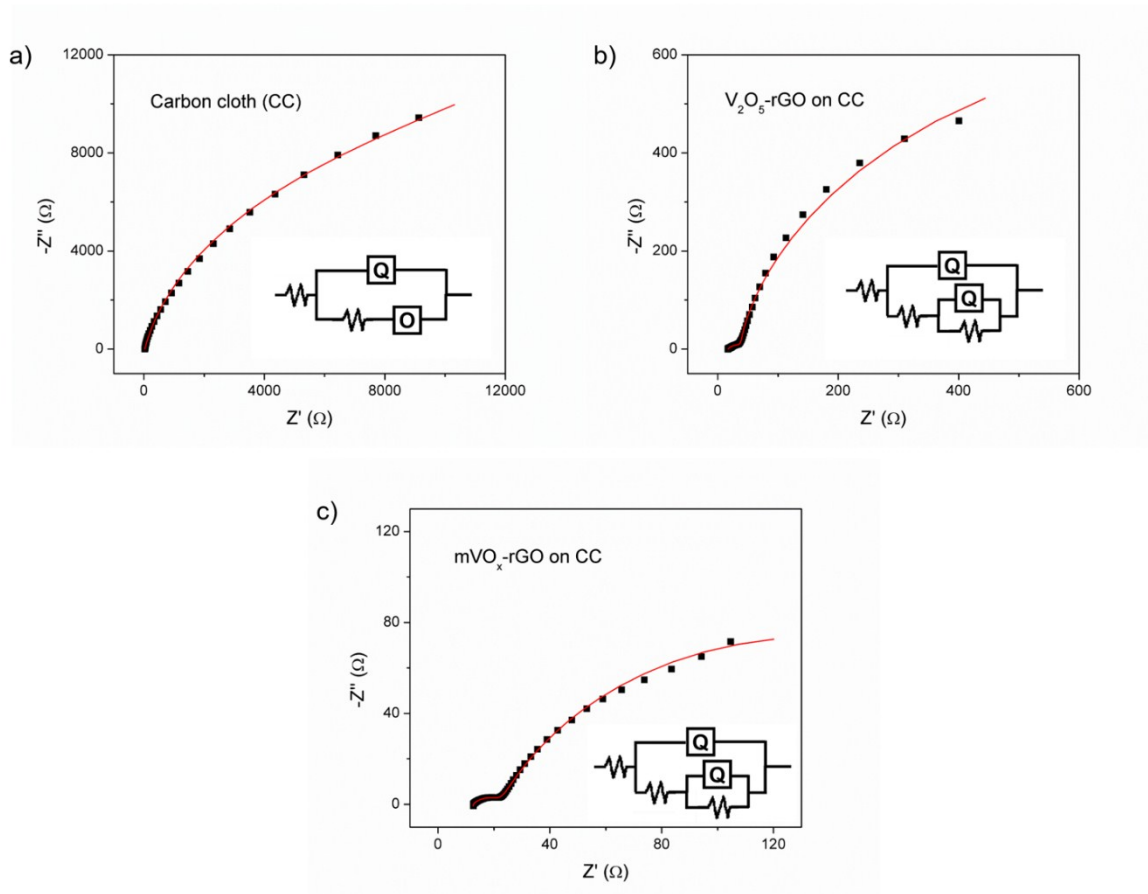


Fig. S3 The fitted EIS spectra of a) carbon cloth, b) V_2O_5 -rGO electrode and c) mVO_x -rGO electrode at open circuit condition.

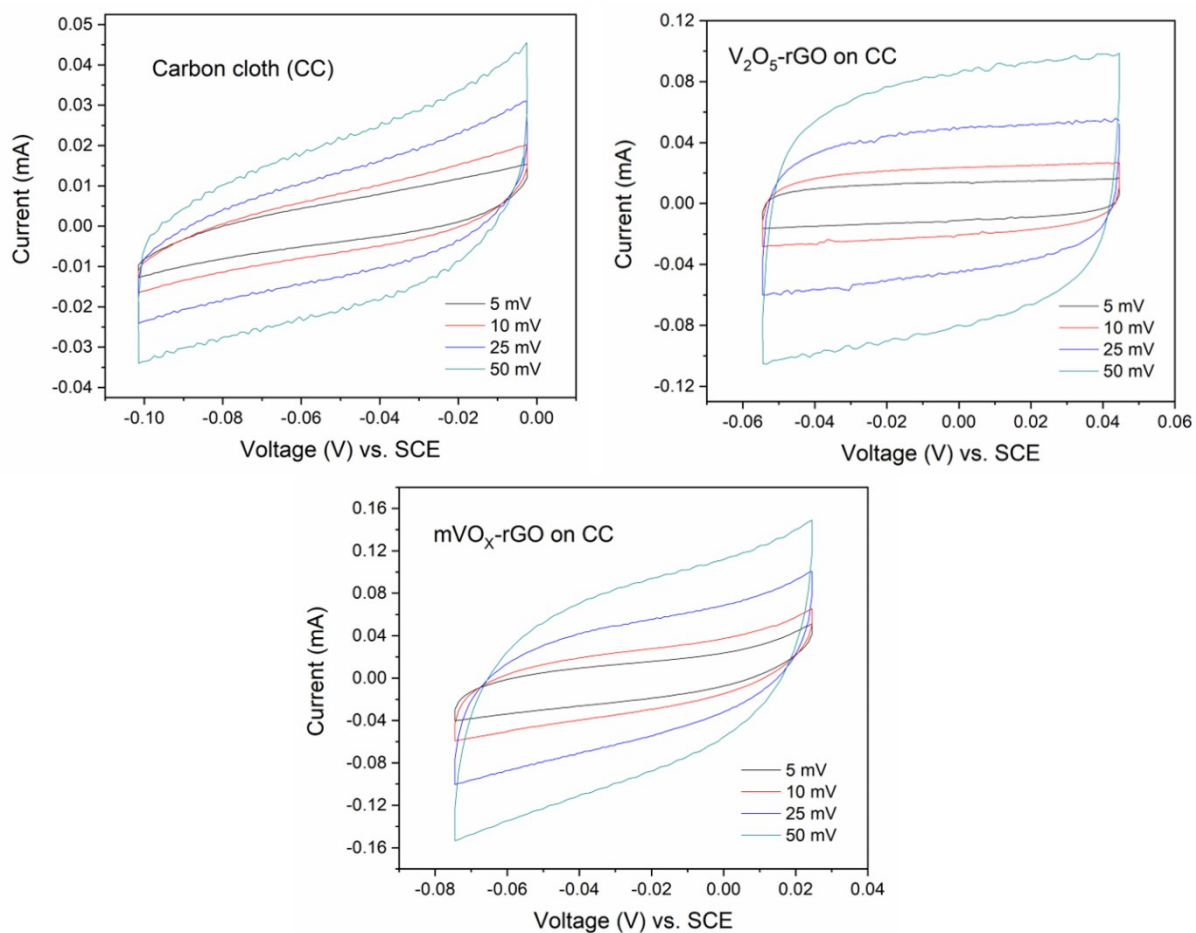


Fig. S4 Cyclic voltammetry curves of a) carbon cloth, b) V_2O_5 -rGO electrode and c) mVO_x -rGO electrode.

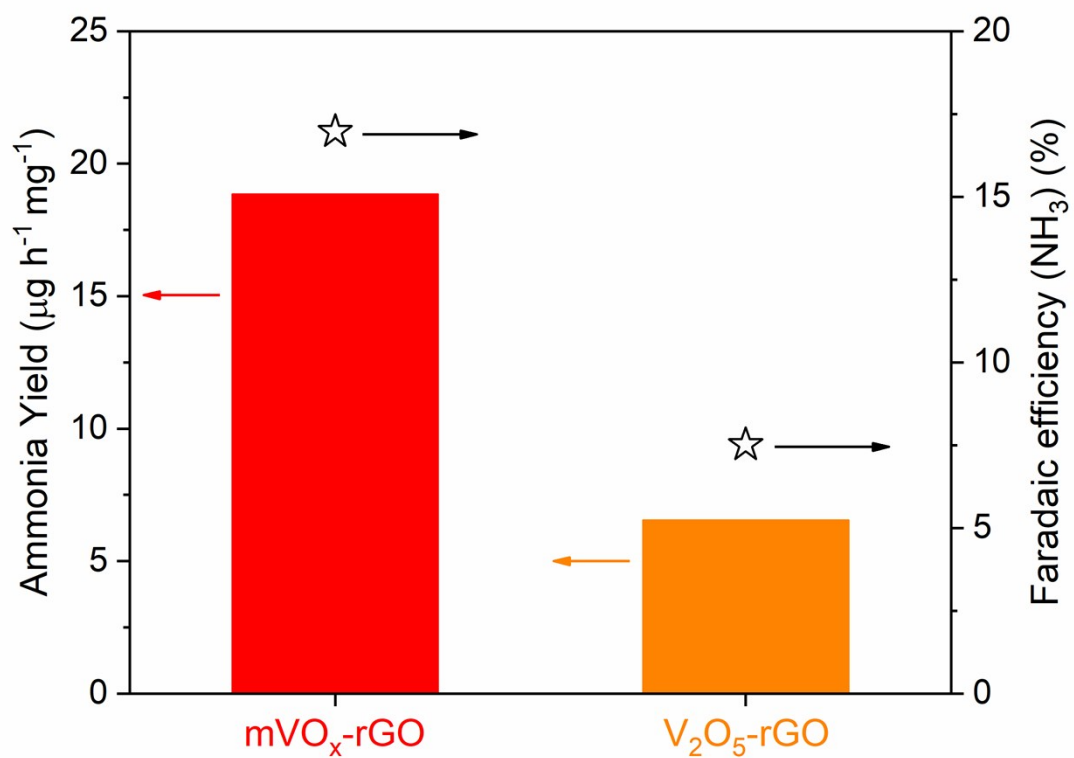


Fig. S5 Ammonia yield and Faradaic efficiency of $\text{mVO}_x\text{-rGO}$ and $\text{V}_2\text{O}_5\text{-rGO}$ at a similar current density of $\sim -0.25 \text{ mA cm}^{-2}$.

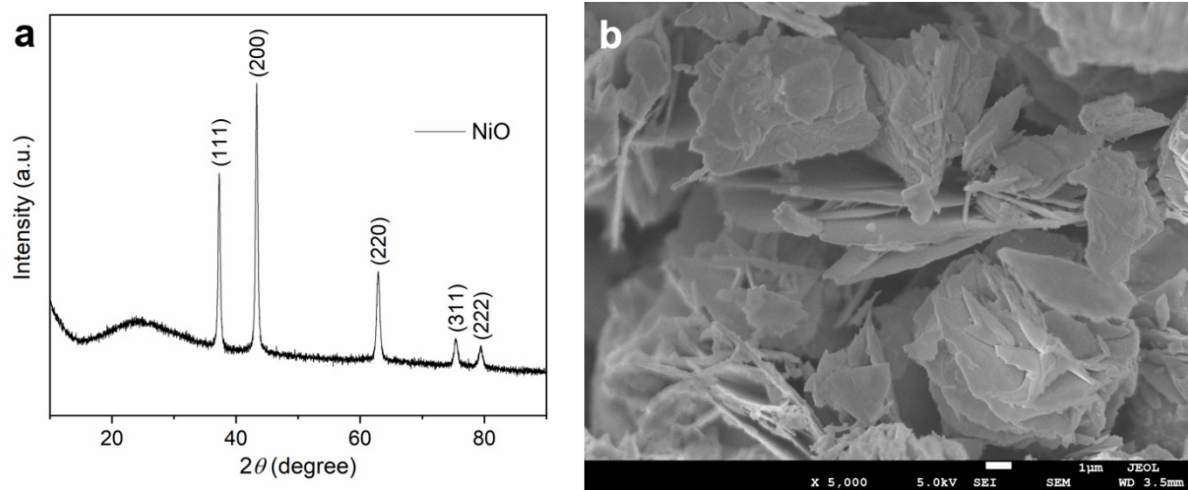


Fig. S6 a) XRD pattern and b) SEM micrograph of NiO nanosheets.

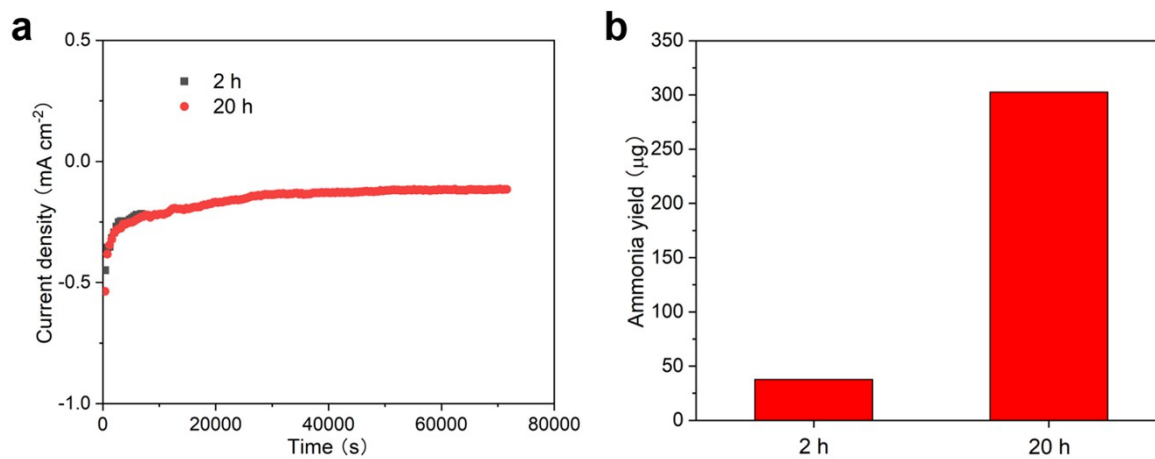


Fig. S7 Time-dependent a) chronoamperometry curves and b) ammonia yields for mVO_x-rGO.

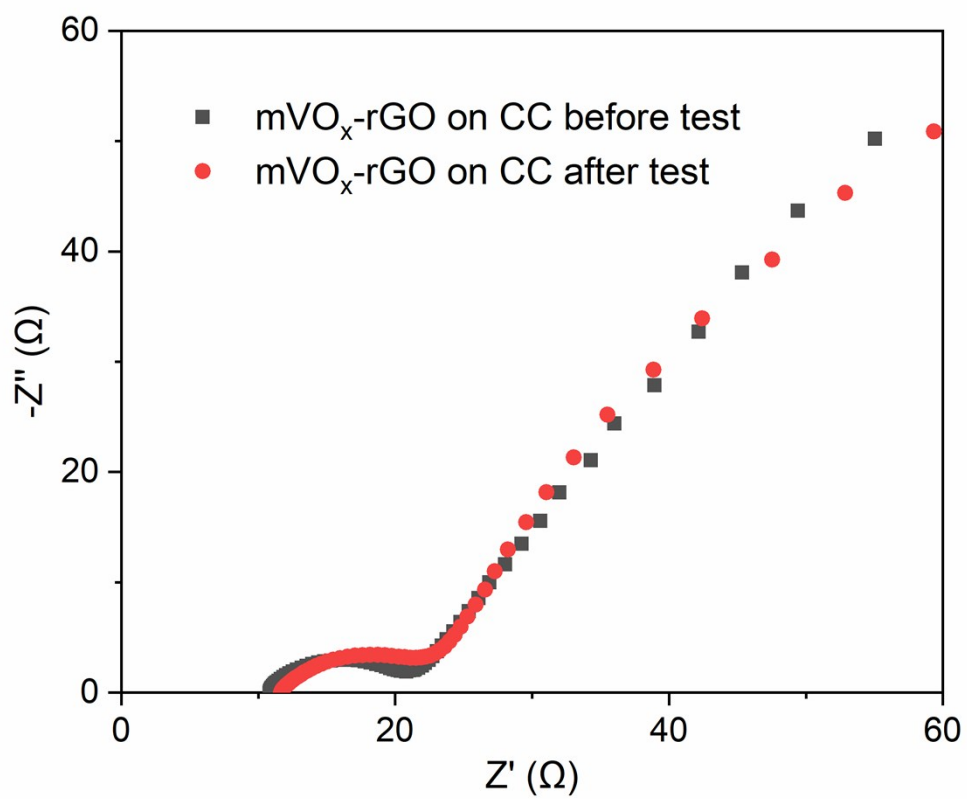


Fig. S8 EIS of mVO_x-rGO electrode before and after 2 h NRR test.

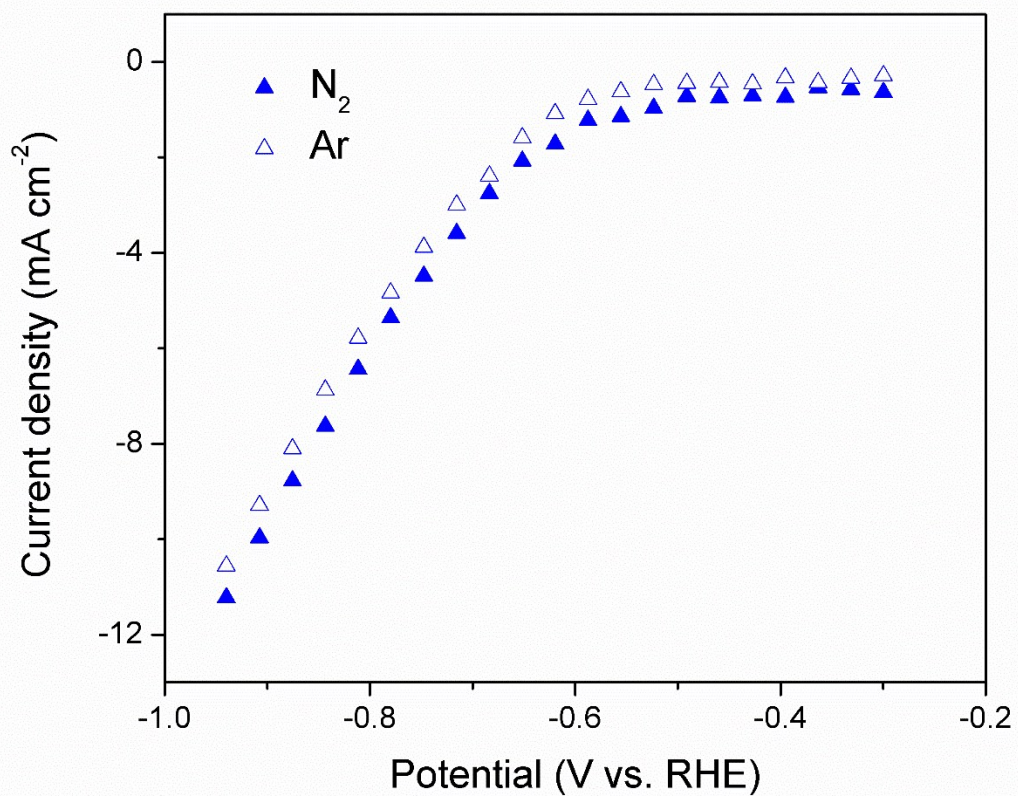


Fig. S9 LSV of mVO_x-rGO electrode in N₂ and Ar saturated 0.1 M Na₂SO₄ electrolyte.

As shown in Fig. S9, the slight difference in LSV curves may come from NRR contribution of mVO_x-rGO.

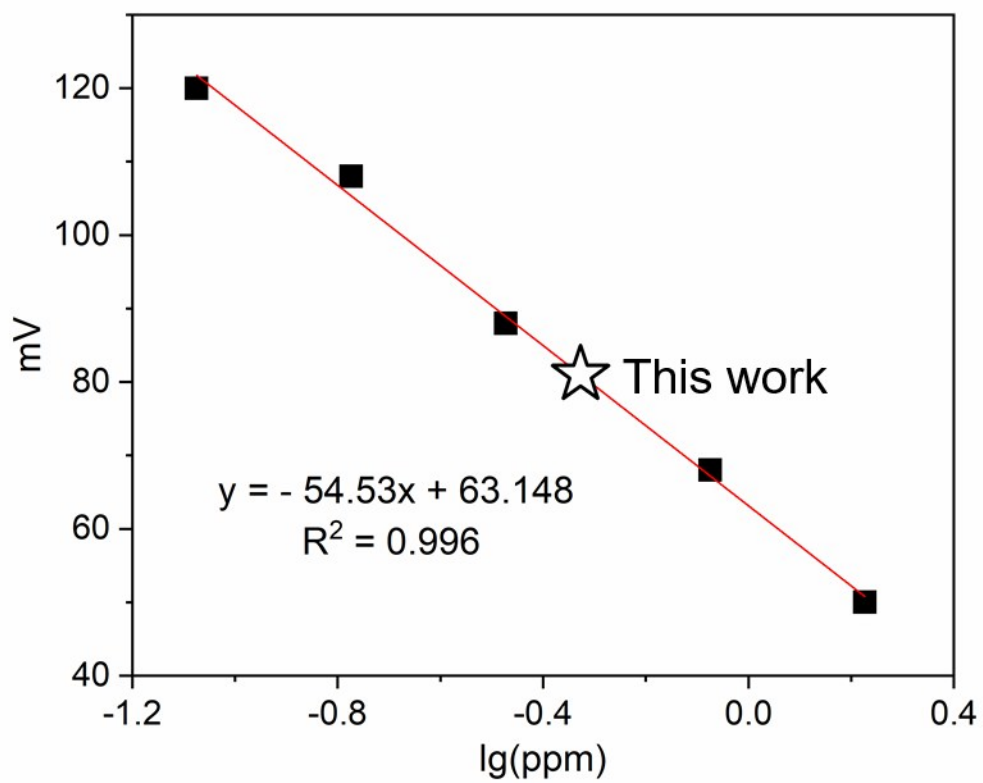


Fig. S10 Calibration of standard NH_4^+ solution detected by the ammonia ion selective electrode.

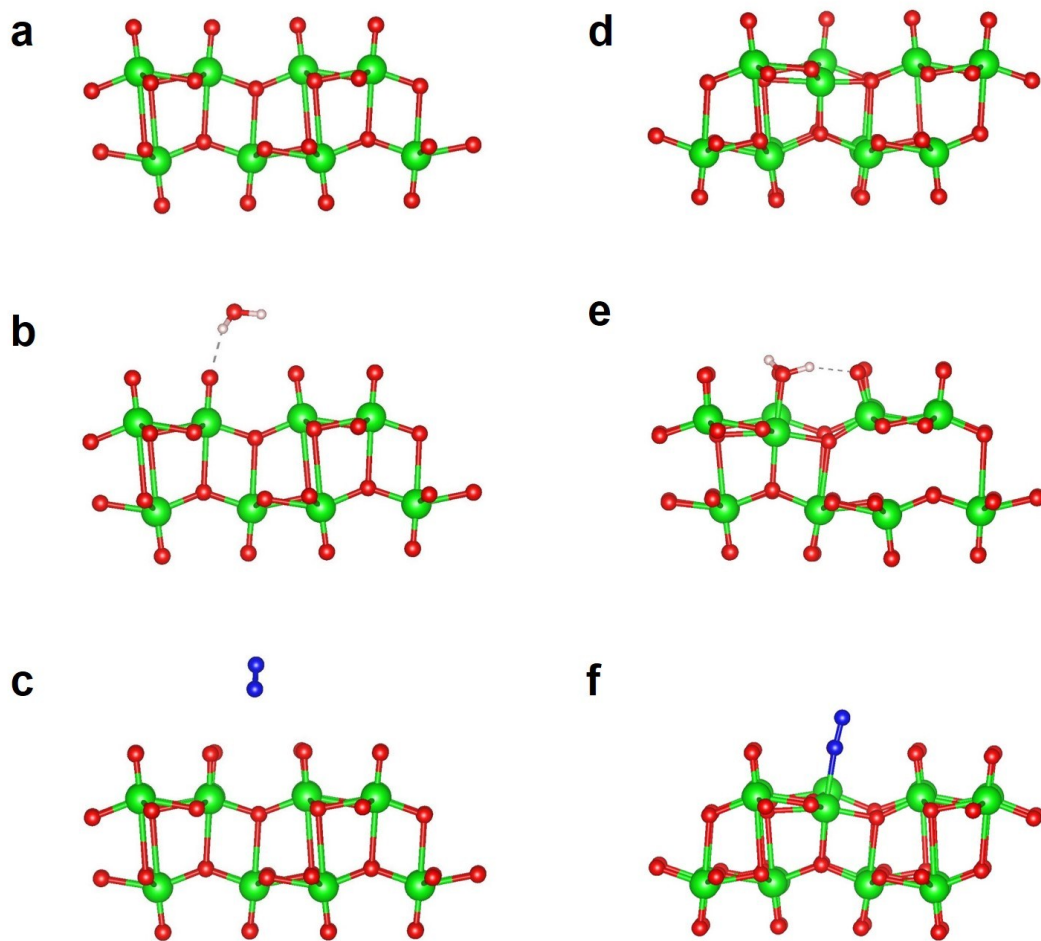


Fig. S11 The optimized structure for a) V_2O_5 , b) H_2O adsorption on V_2O_5 , c) N_2 adsorption on V_2O_5 , d) $mVO_x = V_2O_5$ with oxygen vacancy, e) H_2O adsorption on mVO_x and f) N_2 adsorption on mVO_x . Color code: pink white, H; blue, N; red, O; green, V.

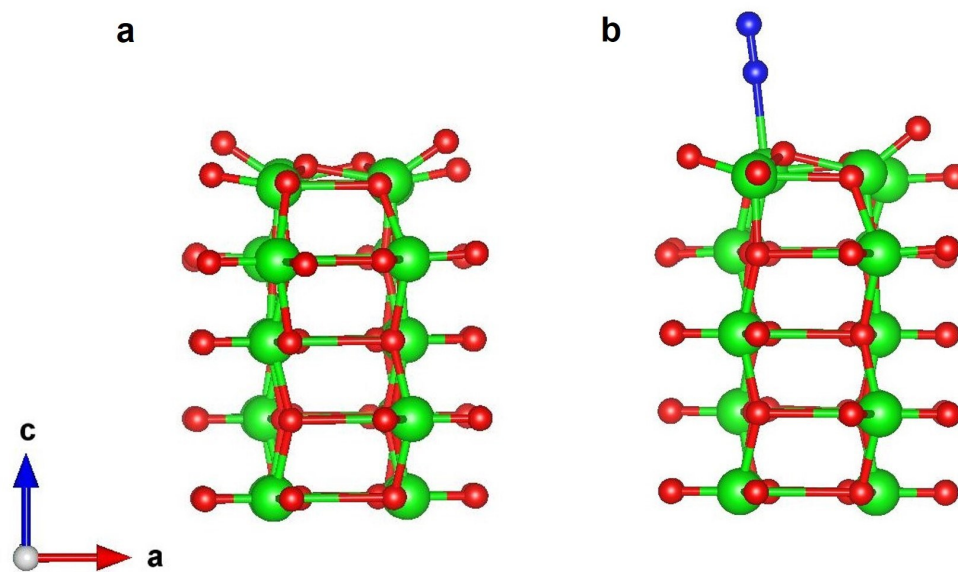


Fig. S12 The optimized structure for a) (010) surface of V₂O₅ and b) N₂ adsorption on (010) surface of V₂O₅. Color code: blue, N; red, O; green, V.

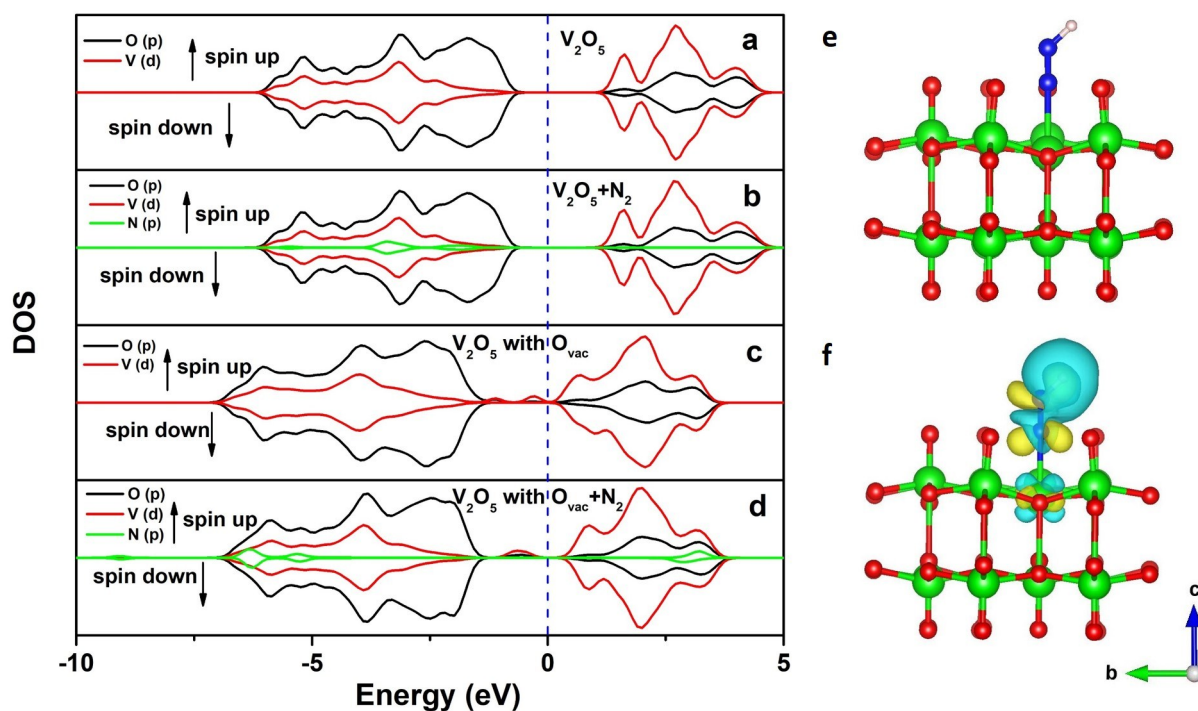


Fig. S13 The density of states for a) V_2O_5 , b) $V_2O_5+N_2$, c) mVO_x (V_2O_5 with O_{vac}) and d) N_2 adsorption on mVO_x (V_2O_5 with O_{vac}). e) The structure of key intermediate of PDS. f) The deformation charge density of $*NNH$, yellow and blue represent charge accumulation and loss, respectively.

It should be noted that the DOS of V_2O_5 is not affected by the N_2 adsorption comparing Fig. S13a and S13b, which indicates that there is no interaction between N_2 and pure V_2O_5 . However, for the V_2O_5 with O_{vac} , the orbital of V is changed at about -5.5 eV with the adsorption of N_2 . The coupled orbital between N and V indicates the N_2 will adsorb on the V site in V_2O_5 with O_{vac} . For the key intermediate of PDS, the deformation charge density of $*NNH$ indicates that the H adsorption will lose the localized bonding electron between N atoms in N_2 . The electron depletion will weaken the bond of N_2 , which is beneficial for the following NRR.

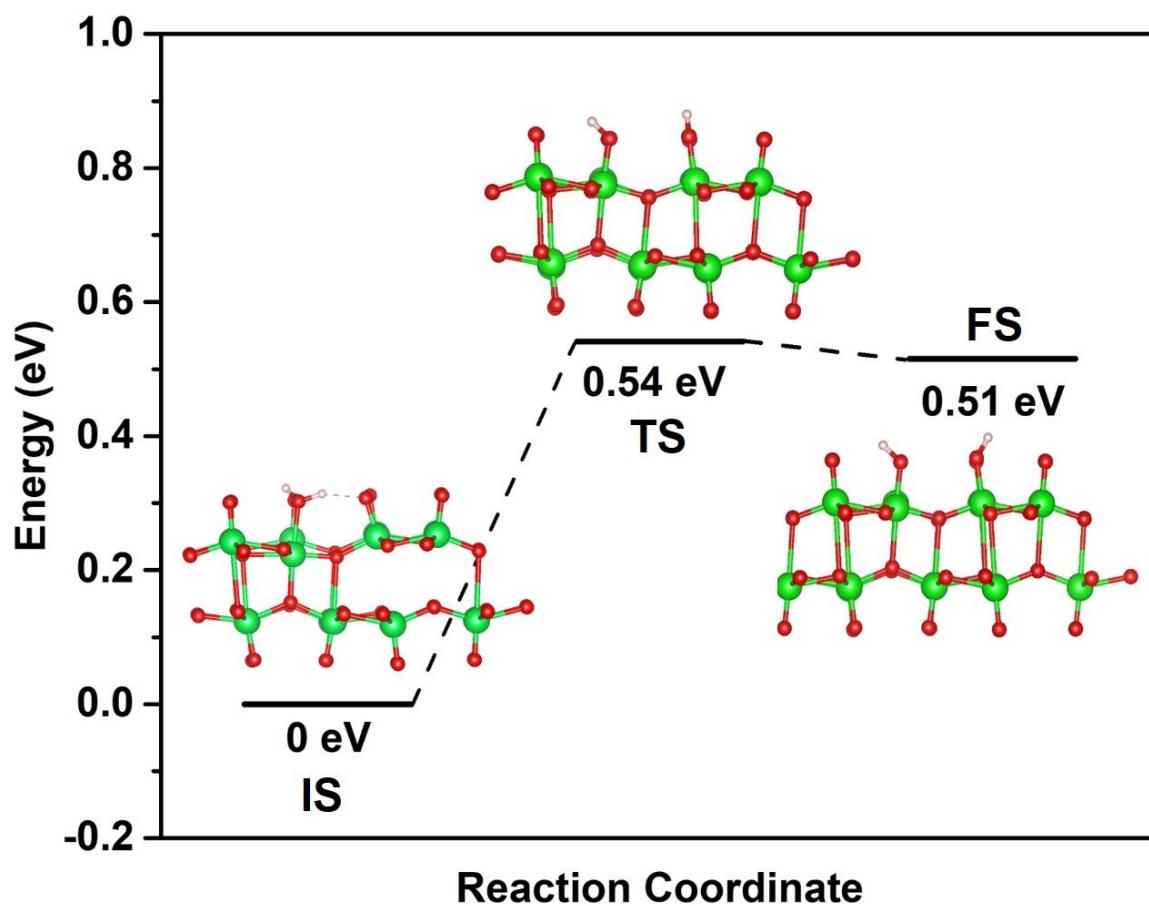


Fig. S14 The calculated energy barrier for H₂O dissociation on mVO_x.

We consider the water adsorption on the V site as the initial state (IS). The H₂O will dissociate to the OH⁻ and H⁺. The OH⁻ will locate on the Ovac site and H⁺ will adsorb on the nearby O atom, which eventually obtained the final state (FS) as shown in Fig. S14. The dissociation energy barrier is 0.54 eV.

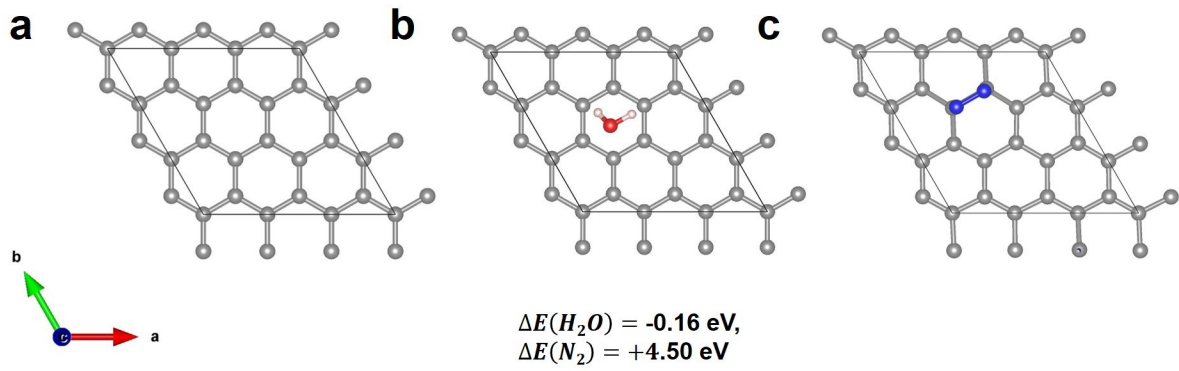


Fig. S15 The optimized structure for (a) graphene, (b) H₂O adsorbed on graphene, (c) N₂ adsorbed on graphene

The adsorption energy of H₂O on graphene is negative (-0.16 eV), which indicates that the H₂O adsorption on graphene is energy favorable. On the contrary, the adsorption energy of H₂O on graphene is very positive (+0.45 eV), which indicates that the N₂ adsorption on graphene is energy unfavorable.

S4. Supporting tables

Applied potential / V	NH ₃ content (cathode electrolyte) / μg	NH ₃ content (anode electrolyte) / μg	NH ₃ content (trapped on Nafion membrane) / μg
-0.35	24	7.33	6.35
-0.45	17.37	7.07	4.92
-0.55	3.02	2.81	0.79
-0.65	2.9	2.74	0.7
-0.75	7.23	3.63	1.92

Table S1 Ammonia content contributed to the anode electrolyte, cathode electrolyte and trapped Nafion membrane respectively at each applied potential by mVO_x-rGO electrode for 2 h of NRR.

The NH₃ content in cathode electrolyte (working electrode side) is always higher than that in anode electrolyte (counter electrode side) since the produced NH₃ can pass through the Nafion membrane, and the result is in consistent with Reference [S16].

Electrocatalyst	Electrolyte	Potential (V vs. RHE)	Faradaic efficiency (%)	Yield rate	Ref.
VN _{0.7} O _{0.45}	Nafion	-0.1	5.95	20.26 $\mu\text{g h}^{-1} \text{cm}^{-2}$	S10
V ₂ O ₃	Nafion	-0.2	0.34	3.30 $\mu\text{g h}^{-1} \text{cm}^{-2}$	S10
VN	0.1M HCl	-0.5	2.25	5.14 $\mu\text{g h}^{-1} \text{cm}^{-2}$	S11
VO ₂	0.1 M Na ₂ SO ₄	-0.7	3.97	14.85 $\mu\text{g h}^{-1} \text{mg}^{-1}$	S12
V-TiO ₂	0.5 M LiClO ₄	-0.4 ^a -0.5 ^b	15.3 ^a	17.73 $\mu\text{g h}^{-1} \text{mg}^{-1\text{b}}$	S13
V ₂ O ₅ -rGO	0.1 M Na ₂ SO ₄	-0.55 ^a -0.75 ^b	7.51 ^a	8.09 $\mu\text{g h}^{-1} \text{mg}^{-1\text{b}}$	This work
mVO _x -rGO	0.1 M Na ₂ SO ₄	-0.35	16.97	18.84 $\mu\text{g h}^{-1} \text{mg}^{-1}$	This work

Table S2 Comparison of NRR performance of various V-containing electrocatalysts.

Catalyst	Electrolyte	Potential (V vs. RHE)	Faradaic efficiency (%)	Yield rate	Ref.
MoS ₂	0.1M Na ₂ SO ₄	-0.5	1.17	4.94 μg h ⁻¹ cm ⁻²	S14
B ₄ C	0.1M Na ₂ SO ₄	-0.65 ^a -0.75 ^b	9.24 ^a	14.70 μg h ⁻¹ mg ⁻¹ ^b	S15
Bi	0.1M Na ₂ SO ₄	-0.8	10.46	13.23 μg h ⁻¹ mg ⁻¹	S16
C@CoS@TiO ₂	0.1M Na ₂ SO ₄	-0.55	28.6	49.51 μg h ⁻¹ cm ⁻²	S17
BP@SnO _{2-x}	0.1M Na ₂ SO ₄	-0.4	14.6	48.87 μg h ⁻¹ mg ⁻¹	S18
Mo ⁰ /GDY	0.1M Na ₂ SO ₄	-0.55	21	145.4 μg h ⁻¹ mg ⁻¹	S19
Pd/C	0.1M PBS	-0.05	2.4	4.9 μg h ⁻¹ mg ⁻¹	S20
Fe/Fe ₃ O ₄	0.1M PBS	-0.3	8.29	0.19 μg h ⁻¹ cm ⁻²	S21
Fe-TiO ₂	0.5M LiClO ₄	-0.4	25.6	25.47 μg h ⁻¹ mg ⁻¹	S22
C-Ti _x O _y /C	0.1M LiClO ₄	-0.4	17.8	14.8 μg h ⁻¹ mg ⁻¹	S23
PEBCD/C	0.5M Li ₂ SO ₄	-0.4 ^a -0.7 ^b	2.91	2.01 μg h ⁻¹ cm ⁻²	S24
mVO _x -rGO	0.1 M Na ₂ SO ₄	-0.35	16.97	18.84 μg h ⁻¹ mg ⁻¹	This work

Table S3 Comparison of the NRR electrocatalytic activity of different catalysts at neutral pH condition.

Reference:

- [S1] G. Kresse and J. Furthmüller, *Phys. Rev. B* 1996, 54, 11169.
- [S2] G. Kresse and J. Hafner, *Phys. Rev. B* 1994, 49, 14251.
- [S3] G. Kresse and J. Hafner, *Phys. Rev. B* 1993, 47, 558.
- [S4] G. Kresse and D. Joubert, *Phys. Rev. B* 1999, 59, 1758.
- [S5] P. E. Blöchl, *Phys. Rev. B* 1994, 50, 17953.
- [S6] V. I. Anisimov, F. Aryasetiawan and A. Lichtenstein, *J. Phys. Condens. Matter* 1997, 9, 767.
- [S7] S. Grimme, *J. Comput. Chem.* 2006, 27, 1787.
- [S8] G. Henkelman, B. P. Uberuaga and H. Jónsson, *J. Chem. Phys.* 2000, 113, 9901.
- [S9] J. Kibsgaard, J. K. Nørskov, I. Chorkendorff, *ACS Energy Lett.* 2019, 4, 2986.
- [S10] X. Yang, J. Nash, J. Anibal, M. Dunwell, S. Kattel, E. Stavitski, K. Attenkofer, J. G. Chen, Y. S. Yan, B. J. Xu, *J. Am. Chem. Soc.* 2018, 140, 13387.
- [S11] R. Zhang, Y. Zhang, X. Ren, G. W. Cui, A. M. Asiri, B. Z. Zheng, X. P. Sun, *ACS Sustainable Chem. Eng.* 2018, 6, 9545.
- [S12] R. Zhang, H. Guo, L. Yang, Y. Wang, Z. Niu, H. Huang, H. Chen, L. Xia, T. Li, X. Shi, X. Sun, B. Li, Q. Liu, *ChemElectroChem* 2019, 6, 1014.
- [S13] T. W. Wu, W. H. Kong, Y. Zhang, Z. Xing, J. X. Zhao, T. Wang, X. F. Shi, Y. L. Luo, X. P. Sun, *Small Methods*, doi: 10.1002/smtd.201900356.
- [S14] L. Zhang, X. Q. Ji, X. Ren, Y. J. Ma, X. F. Shi, Z. Q. Tian, A. M. Asiri, L. Chen, B. Tang, X. P. Sun, *Adv. Mater.* 2018, 30, 1800191.
- [S15] W. B. Qiu, X. Y. Xie, J. D. Qiu, W. H. Fang, R. P. Liang, X. Ren, X. Q. Ji, G. W. Cui, A. M. Asiri, G. L. Cui, B. Tang, X. P. Sun, *Nat. Commun.* 2018, 9, 3485.
- [S16] L. Q. Li, C. Tang, B. Q. Xia, H. Y. Jin, Y. Zheng, S. Z. Qiao, *ACS Catal.* 2019, 9, 2902.
- [S17] B. Ding, Y. T. Liu, X. X. Chen, J. Y. Yu, *Angew. Chem. Int. Ed.* 2019, doi.org/10.1002/anie.201912733.
- [S18] Y. T. Liu, D. Li, J. Y. Yu, B. Ding, *Angew. Chem. Int. Ed.* 2019, doi.org/10.1002/ange.201908415.
- [S19] L. Hui, Y. R. Xue, H. D. Yu, Y. X. Liu, Y. Fang, C. Y. Xing, B. L. Huang, Y. L. Li, *J. Am. Chem. Soc.* 2019, 141, 10677.
- [S20] J. Wang, L. Yu, L. Hu, G. Chen, H. L. Xin, X. F. Feng, *Nat. Commun.* 2018, 9, 1795.
- [S21] L. Hu, A. Khaniya, J. Wang, G. Chen, W. E. Kaden, X. F. Feng, *ACS Catal.* 2018, 8, 9312.

[S22] T. W. Wu, Z. Xing, S. Y. Mou, C. B. Li, Y. X. Qiao, Q. Liu, X. J. Zhu, Y. L. Luo, X. F. Shi, Y. N. Zhang, X. P. Sun, *Angew. Chem. Int. Ed.* 2019, doi.org/10.1002/anie.201911153.

[S23] Q. Qin, Y. Zhao, M. Schmallegger, T. Heil, J. Schmidt, R. Walczak, G. G. Demner, H. J. Jiao, M. Oschatz, *Angew. Chem. Int. Ed.* 2019, 58, 13101.

[S24] G. F. Chen, X. R. Cao, S. Q. Wu, X. Y. Zeng, L. X. Ding, M. Zhu, H. H. Wang, *J. AM. Chem. Soc.* 2017, 139, 9771.